Okuda and Ide *Earth, Planets and Space (2018) 70:132*
https://doi.org/10.1186/s40623-018-0903-8

Earth, Planets and Space

FULL PAPER Open Access

Streak and hierarchical structures of the Tohoku–Hokkaido subduction zone plate boundary

Takashi Okuda and Satoshi Ide*

Abstract

Here, we investigated four families of moderate-size ($M \sim 4.8$) repeating earthquakes and nearby smaller events that occurred in the Naka-Oki, Kushiro-Oki, Urakawa-Oki, and Kamaishi-Oki regions of the Tohoku–Hokkaido subduction zone, Japan, between 2002 and 2017. We employed a hypocenter relocation method based on waveform cross-correlations of the above four families, as well as a waveform inversion method using the empirical Green's function for the Naka-Oki and Kushiro-Oki earthquakes, where every moderate-size repeating earthquake showed complex and variable rupture processes. However, their rupture areas overlapped significantly and were elongate parallel to the slip direction. Some parts of these areas were also repeatedly ruptured by smaller earthquakes, with these smaller earthquakes and moderate events sometimes following almost identical rupture processes. The results indicate the existence of a characteristic structure that is represented by several elliptical patches that are elongate in the slip direction of the plate interface. It is likely that many streak structures have developed over a 1000 km along-strike section of the plate interface that extends from the Kushiro-Oki region to the Naka-Oki region of the subduction zone. These patches may be distributed hierarchically, with the smaller patches rupturing independently. The rupture of a smaller patch may either stop, producing a small earthquake, or it may grow into a large earthquake, with this rupture process depending on subtle differences in the physical conditions that we are unable to observe in a practical sense. Earthquakes are random processes, but they may not be completely random, as the preexisting characteristic structure of the seismic region may control the rupture process to some degree.

Keywords: Repeating earthquake, Waveform inversion, Streak structure, Hierarchical structure

Introduction

Earthquakes are dynamic rupture phenomena along a fault that begin as small ruptures. Most ruptures are short-lived, resulting in small earthquakes, whereas some continue to propagate into large earthquakes. It has been debated whether the size of an earthquake can be characteristically determined or if it is a random process in a given seismogenic region, with inferences regarding the evolution of an earthquake lying between the two end-members of the conceptual earthquake rupture model: the characteristic model and the hierarchical model.

Reactivation of the same rupture source along a fault has been previously reported, which suggests that it is possible to determine the earthquake size from certain seismogenic regions. We term this earthquake behavior "characteristic". Many moderate to large earthquakes behave characteristically to some extent, such as the $M8$ Tokachi-Oki (Yamanaka and Kikuchi 2003), $M7$ Ibaraki-Oki (Mochizuki et al. 2008; Matsumura 2010), $M6$ Parkfield (Bakun and Lindh 1985), and $M5$ Kamaishi-Oki events (Okada et al. 2003; Shimamura et al. 2011; Uchida et al. 2012). Moreover, small repeating earthquakes are detected globally, such as those in California (Nadeau and Johnson 1998; Nadeau and McEvilly 1999), the Tohoku–Hokkaido subduction zone (Matsuzawa 2002; Igarashi et al. 2003; Matsubara et al. 2005), Kanto

*Correspondence: ide@eps.s.u-tokyo.ac.jp
Department of Earth and Planetary Science, University of Tokyo, Tokyo, Japan

(Matsuzawa 2002; Igarashi et al. 2003), Ryukyu (Igarashi 2010; Yamashita et al. 2012), Turkey (Peng and Ben-Zion 2005), and Taiwan (Chen et al. 2008). These characteristic earthquakes suggest the existence of a time-independent patch-like structure that is embedded on the plate boundary and forms the basis of the characteristic earthquake model. The potential earthquake size is determined characteristically for each seismic region as a function of the size of the patch.

However, it is well known that many natural earthquakes show various types of scale independence (Kanamori and Anderson 1975; Ide and Beroza 2001) and a power-law distribution (Gutenberg and Richter 1944). Some studies also report a self-similarity at the very beginning of the seismic waveforms that is independent of earthquake size (Abercrombie and Mori 1994; Mori and Kanamori 1996; Uchide and Ide 2010; Meier et al. 2016). These observations suggest a large degree of self-similarity, which forms the basis of the hierarchical earthquake model, where the earthquake rupture propagates as a cascading failure of hierarchical patch-like structures over a range of scales and without any distinguishable nucleation process (Ellsworth and Beroza 1995; Ide and Aochi 2005). In this case, the final earthquake size is random.

The rupture process can vary from event to event during the repetitive rupture of the same patch along the fault interface, as has often been suggested for both large interplate events (Yamanaka and Kikuchi 2004; Bakun et al. 2005; Wu et al. 2008) and small to moderate repeating earthquakes (Shimamura et al. 2011; Uchida et al. 2015). Most of these earthquakes have properties that are intermediate between those of the characteristic and hierarchical models, and are highly variable. However, there is no quantitative measure for determining the characteristic and hierarchical nature of the source, such that this characterization of the earthquake rupture process is still qualitative owing to insufficient observations of the repetitive ruptures in specific study regions. We can therefore seek to increase our understanding of these rupture processes by conducting detailed investigations of such repetitive event sequences.

Moderate-size repeating earthquakes are ideal targets for a comprehensive analysis of the regional characteristics of rupture processes. Several repeating $M \sim 4.8$ earthquake sequences have been observed in the Tohoku–Hokkaido subduction zone, Japan (Uchida and Matsuzawa 2013). We therefore investigated four families of moderate-size ($M \sim 4.8$) repeating earthquakes and nearby smaller events that occurred in the Naka-Oki, Kushiro-Oki, Urakawa-Oki, and Kamaishi-Oki regions between 2002 and 2017. These moderate-size repeating earthquakes occurred near the coast, relatively close to the dense coverage of the inland seismic stations (Fig. 1), most of which are Hi-net stations from the high-sensitivity seismic observation network operated by the National Research Institute for Earth Science and Disaster Resilience (NIED) of Japan since 2002. This continuous 15-year record of seismicity along the Tohoku–Hokkaido subduction zone provides an ideal opportunity to investigate variations in the rupture processes of moderate-size repeating earthquakes.

The remainder of this manuscript is organized as follows. In section "Overall properties of the moderate-size earthquakes", we present accurate relative source locations in the Naka-Oki, Kushiro-Oki, Urakawa-Oki, and Kamaishi-Oki regions to better understand the seismogenic characteristics over large time and magnitude ranges. The seismicity of the Urakawa-Oki and Kamaishi-Oki regions occurs along streak structures on the plate interface that are oriented parallel to the direction of fault slip. In section "Estimating the earthquake rupture processes", we investigate the detailed source processes of the earthquakes in the Naka-Oki and Kushiro-Oki regions using an empirical Green's function (eGf). The final slip distribution is elongate in the slip direction, whereas the streaks in seismicity are not clear in these regions. We further discuss this slip evolution in section "Characteristics of the rupture process", which suggests a hierarchical structure. Finally, concluding remarks are presented in section "Conclusion."

Overall properties of the moderate-size earthquakes

We determined the accurate relative locations of the source centroids for 61, 16, 115, and 85 earthquakes in the Naka-Oki, Kushiro-Oki, Urakawa-Oki, and Kamaishi-Oki regions, respectively, using the relative arrival times determined by waveform cross-correlations (Ohta and Ide 2008, 2011). This method consists of two steps. We first estimated the relative hypocenter locations for each pair of events by maximizing the summation of the waveform cross-correlations for all the stations and seismogram components and then determined the set of centroids that were consistent with the relative locations in a least-squares sense, weighted using the value of the summed cross-correlations (Ohta and Ide 2008, 2011). The analyzed data consist of velocity seismograms recorded at 72, 115, 132, and 296 stations in the Naka-Oki, Kushiro-Oki, Urakawa-Oki, and Kamaishi-Oki regions, respectively, selected from 404 stations (a combination of Hi-net, Japan Metrological Agency (JMA), The University of Tokyo, Hokkaido University, and Tohoku University stations). Each seismic station is equipped with a 1-Hz 3-component seismometer that records the ground velocity at 100 samples per

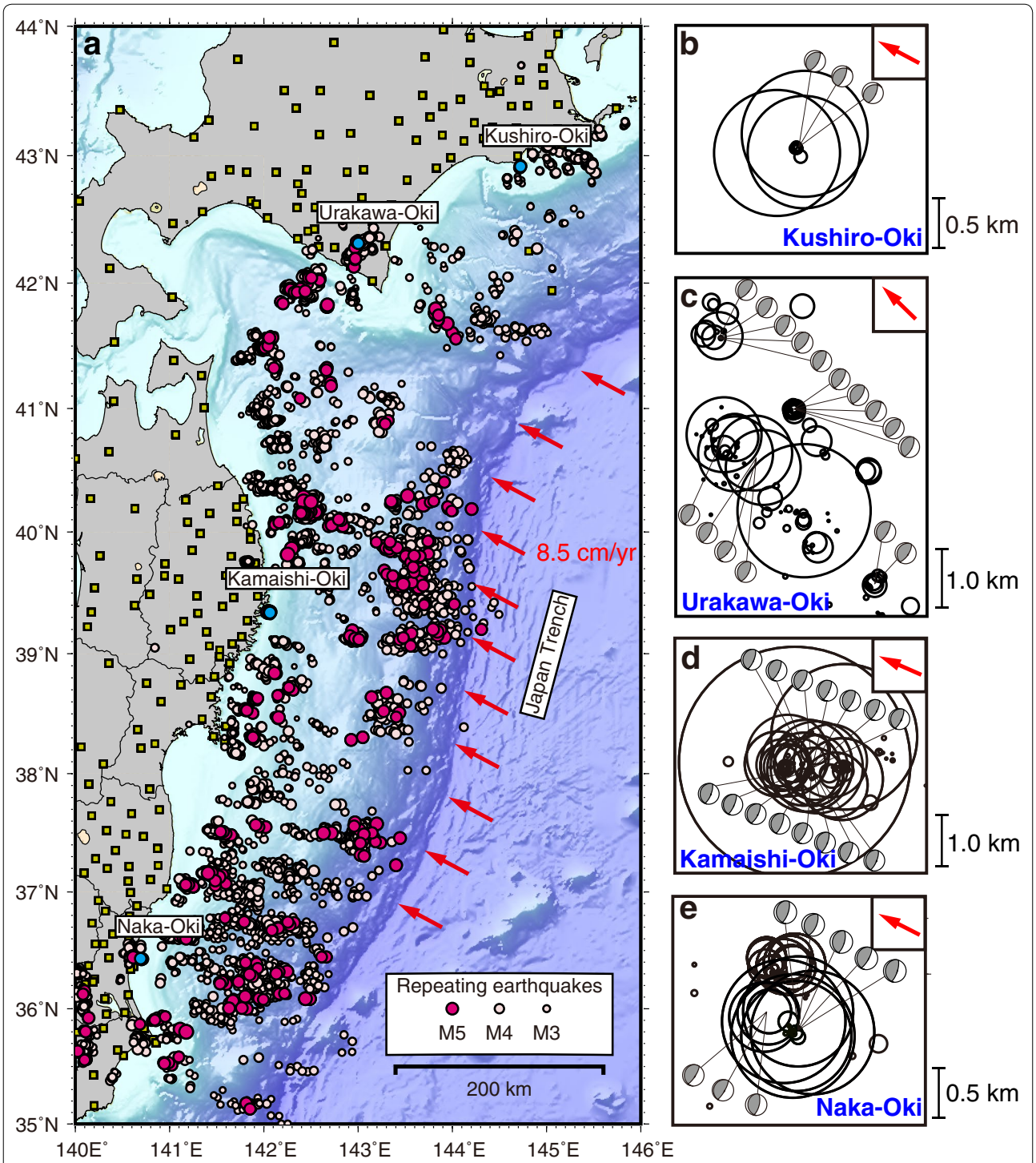

Fig. 1 Moderate-size repeating earthquakes in the Tohoku–Hokkaido subduction zone. **a** Locations of repeating earthquakes. The magenta circles show repeating earthquakes (Uchida and Matsuzawa 2013), and cyan circles indicate the four studied repeating earthquake sequences. The yellow squares show the stations used in the relocation analysis. **b**–**e** Centroid locations (circles) for the repeating earthquakes in the Kushiro-Oki (**b**), Urakawa-Oki (**c**), Kamaishi-Oki (**d**), and Naka-Oki (**e**) regions, with the radius of each circle representing the expected source size. The beach balls give the focal mechanisms of selected events. The red arrows indicate the averaged slip direction that was determined from the focal mechanisms in each region

second. A 1–10 Hz bandpass filter was applied to the data prior to the analysis. The waveform cross-correlations were computed using a 4-s window that began 1 s before the onset of the P-wave and S-wave arrivals.

Figure 1 shows the relocated centroid distributions of the repeating earthquakes in the four study regions. The estimated values for each event are summarized in Additional file 1: Tables S1–S4. Each panel of Fig. 1b–e shows the earthquake locations as circles, with the circle sizes representing the estimated source sizes for the events that were calculated from their magnitudes and a constant stress drop of 38 MPa, which was estimated for the Kamaishi-Oki repeating earthquake sequence (Matsuzawa 2002; Uchida et al. 2012). The estimated errors in the source locations vary and are dependent on the individual earthquakes, but the average standard deviations are 100, 200, 20, and 70 m in the Naka-Oki, Kushiro-Oki, Urakawa-Oki, and Kamaishi-Oki regions, respectively. The focal mechanisms determined by the NIED for the $M>3.5$ earthquakes are indicative of low-angle reverse faults, thus highlighting that these events occurred along the plate boundary.

The earthquake centroids in the Urakawa-Oki and Kamaishi-Oki regions are linearly distributed and oriented parallel to the regional slip direction (red arrow in Fig. 1b–e), as estimated from the focal mechanisms in each region. While this feature is not clear in the seismicity of the Naka-Oki and Kushiro-Oki regions, we image another type of streak-like structure that is parallel to the slip direction by employing the slip inversion described in the following section.

Most of these earthquakes have been recognized as repeating earthquakes that consistently rupture approximately the same patch of the plate interface (Uchida and Matsuzawa 2013). We divided the analyzed earthquakes into several groups based on this information and the relocation results. Four groups (M, A, B, and C) were defined in the Naka-Oki region to represent the $\sim M4.8$, $\sim M4$, $\sim M3$, and $\sim M2$ events, respectively (Fig. 2a). Two groups (M and D) were defined in the Kushiro-Oki region to represent the $\sim M4.8$ and $\sim M3$ events, respectively (Fig. 2b). The relative locations, expected source sizes, and possible errors suggest that the rupture areas of earthquakes in each group were likely to overlap. Furthermore, the rupture areas of the group M events

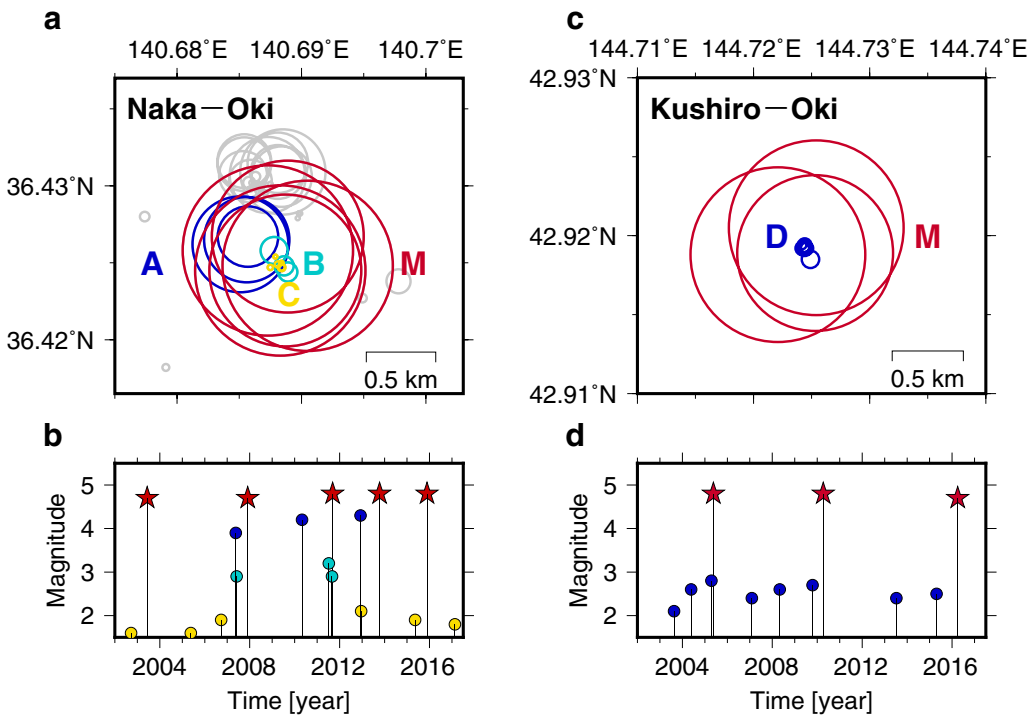

Fig. 2 Moderate-size repeating earthquakes in the Kushiro-Oki and Naka-Oki regions. **a** Earthquake distribution in the Naka-Oki region. The center and size of each circle represent the centroid location and estimated source size, respectively. The red, blue, cyan, and yellow circles indicate the group M, A, B, and C events, respectively. Gray circles show ungrouped events. **b** Magnitude–time diagram of the group M, A, B, and C events. **c** Earthquake distribution in the Kushiro-Oki region. The red and blue circles indicate group M and D events, respectively. **d** Magnitude–time diagram of the group M and D events

include the rupture areas of the smaller events in each region (groups A, B, and C for the Naka-Oki region, and group D for the Kushiro-Oki region), which suggests the existence of hierarchical structures embedded on the plate interface.

Estimating the earthquake rupture processes

Empirical waveform inversion method

We conduct an inversion analysis to determine the spatiotemporal distribution of slip on an assumed fault plane (Ide and Takeo 1997; Ide 2001). A general representation of the slip distributions is expanded using the 2-D spatial and temporal basis functions, with the expansion coefficients being unknown parameters. The spatiotemporal distribution of slip rate $\dot{u}(\boldsymbol{\xi}, \tau)$ is expressed as:

$$\dot{u}(\boldsymbol{\xi}, \tau) = \sum a_{lmn} \phi_l^1(\xi_1) \phi_m^2(\xi_2) \psi_n(\tau), \tag{1}$$

where a_{lmn} are the expansion coefficients, and $\phi_l^1(\xi_1)$, $\phi_m^2(\xi_2)$, and $\psi_n(\tau)$ are the basis functions in the strike direction, dip direction, and over time, respectively. The slip direction is assumed to be unique to the fault. Here, each basis function is a linear B-spline with a triangular shape that is determined by three knots, which yields a continuous spatiotemporal slip distribution in principle.

The relation between the synthetic displacement at station $u_j(\boldsymbol{x}, t)$ and the slip rate distribution on fault $\dot{u}(\boldsymbol{\xi}, \tau)$ is represented as:

$$u_j(\boldsymbol{x}, t) = \iint g_j(\boldsymbol{x}, t; \boldsymbol{\xi}, \tau) \dot{u}(\boldsymbol{\xi}, \tau) \mathrm{d}\boldsymbol{\xi}\, \mathrm{d}\tau, \tag{2}$$

where $g_j(\boldsymbol{x}, t; \boldsymbol{\xi}, \tau)$ is the jth component of the synthetic displacement when an impulsive slip rate is applied at $\boldsymbol{x} = \boldsymbol{\xi}$ and $t = \tau$ (e.g., Aki and Richards 1980). The eGf approach assumes that the waveforms from a small earthquake (eGf event) approximate the point dislocation response from points near the source of the eGf event once the appropriate time shift due to the location difference is taken into account. An advantage of this method over theoretical waveform computation is that we do not have to model the effects of complex Earth structure. If we use the jth component of the displacement record of an event, $G_j(t)$, for the eGf, $g_j(\boldsymbol{x}, t; \boldsymbol{\xi}, \tau)$ is then represented as:

$$g_j(\boldsymbol{x}, t; \boldsymbol{\xi}, \tau) = \frac{1}{M_o^s} G_j\big(t - (t_t - t_k) - T(\boldsymbol{x}, \boldsymbol{\xi}) + T\big(\boldsymbol{x}, \boldsymbol{\xi}^s\big)\big) \frac{R\big(\boldsymbol{x}, \boldsymbol{\xi}^s\big)}{R(\boldsymbol{x}, \boldsymbol{\xi})}, \tag{3}$$

where t_t and t_k represent the origin time of the target and eGf events, respectively; $\boldsymbol{\xi}^s$ and M_o^S are the source location and seismic moment of the eGf event, respectively; $T(\boldsymbol{x}, \boldsymbol{\xi})$ is the theoretical travel time of the P-wave or S-wave from $\boldsymbol{\xi}$ to $\boldsymbol{x}$; $R(\boldsymbol{x}, \boldsymbol{\xi})$ is the distance between $\boldsymbol{\xi}$ and $\boldsymbol{x}$, which is used to account for the geometrical spreading effect; and M_o^s is the seismic moment of the eGf event, which is calculated from its magnitude in the JMA catalog. The source time function of the eGf event in Eq. (3) is assumed to be a delta function, which is not exactly true. The data are convolved with an assumed source time function that takes the small but finite source duration of the eGf event into account, which is an isosceles-triangle-shaped function whose duration is estimated using the records from nearby stations. Since all the eGf events used in this study were of similar size, M2.7–2.9, we always assumed that the duration is 0.1 s.

An equation with the observed displacement $u_j^0(\boldsymbol{x}, t)$ is obtained from Eqs. (1)–(3) as:

$$u_j^0(\boldsymbol{x}, t) = \sum a_{lmn} \iint g_j(\boldsymbol{x}, t; \boldsymbol{\xi}, \tau) \phi_l^1(\xi_1) \phi_m^2(\xi_2) \psi_n(\tau) \mathrm{d}\boldsymbol{\xi}\, \mathrm{d}\tau + e_j(\boldsymbol{x}, t), \tag{4}$$

where $e_j(\boldsymbol{x}, t)$ is the error between the observed and synthetic displacement. This equation is rewritten in vector form as:

$$\boldsymbol{d} = \boldsymbol{G}\boldsymbol{m} + \boldsymbol{e}, \tag{5}$$

where $\boldsymbol{d}$, $\boldsymbol{m}$, and $\boldsymbol{e}$ are the data vectors that contain the sampled data $u_j^0(x, t)$, the a_{lmn} parameters, and the errors $e_j(x, t)$, respectively; $\boldsymbol{G}$ is an $N \times M$ matrix, where N is the number of data and M is the number of parameters, which is obtained after performing the integration in Eq. (4). It should be noted that the error vector $\boldsymbol{e}$ contains both measurement and modeling errors, such as the inaccuracy of the underground structure to compute travel times and a simple assumption of the fault plane geometry. The maximum likelihood estimates of model parameters $\boldsymbol{m}^{\boldsymbol{MLE}}$ are obtained as:

$$\boldsymbol{m}^{\boldsymbol{MLE}} = \left(\boldsymbol{G}^t \boldsymbol{G}\right)^{-1} \boldsymbol{G}^t \boldsymbol{d} \tag{6}$$

for the case where $e_j(x, t)$ has an independent and unbiased Gaussian distribution (e.g., Menke 2012). Equation (6) generally yields a solution that includes many negative parameters, which we consider unnatural. Therefore, we adopt the nonnegative least squares (NNLS) algorithm of Lawson and Hanson (1984) to determine a part of the parameter sets, $\boldsymbol{m}^{\boldsymbol{NNLS}}$, which has a positive value:

$$\boldsymbol{m}^{NNLS} = \left(\boldsymbol{G}'^{t}\boldsymbol{G}'\right)^{-1}\boldsymbol{G}'^{t}\boldsymbol{d}, \tag{7}$$

where $\boldsymbol{G}'$ is a matrix consisting of rows that correspond to $\boldsymbol{m}^{NNLS}$. We performed this slip inversion without a priori constraints on the initial rupture point, rupture velocity, and smoothness of the solution.

The strike and dip angles of the fault plane were assumed based on the NIED F-net focal mechanisms (Fig. 1). The model space is defined as an approximately 1 km × 1 km region on this focal plane, with the exact size being empirically determined for each event through preliminary analyses to cover the major slip region of each event. The temporal model space is also empirically determined. We applied a 1–8 Hz bandpass filter to the vertical component of the P-wave and the north–south and east–west components of the S-wave ground velocity seismograms. The data length is determined to include all signals with sufficient margins. 1.8-s and 2.0-s records are used for group M events in the Kushiro-Oki and Naka-Oki regions, respectively, while shorter data are used for smaller events. Each data begin 0.3 s before the onset of either the P- or S-wave arrivals. Data that are degraded by high noise levels are not used in this analysis (Additional file 1: Figure S1).

The model error was estimated using the bootstrap method (Efron and Tibshirani 1994). We randomly resampled the same number of stations used in the analysis, allowing for duplication of the same data, and re-estimated the model parameters using the NNLS. This procedure was then repeated many times, with the mean and standard deviation of the model parameters calculated after each trial. This allowed us to also evaluate the mean and errors in the quantities that shape the rupture process, such as the total seismic moment, cumulative slip distribution, slip rate history, and source time functions, by calculating the mean and standard deviation of these values from the model parameters estimated from all the trials. Figure 3 demonstrates how the slip distribution and model errors converge to the final solution. The mean and errors do not change significantly after 100 trials, with a fairly smooth slip distribution obtained without having to explicitly introduce smoothing constraints. Therefore, to save computational time, we obtained the final solution using at least 100 bootstrap samples in each of the following analysis.

Results of the Kushiro-Oki slip inversion

We determined the spatiotemporal slip distribution for three *M*4.7–4.8 earthquakes and a small group D earthquake (Table 1, Additional file 1: S5) in the Kushiro-Oki region. Figure 4 compares the observed and modeled M2005 waveforms (group M earthquake that occurred in 2005), with D2005 used as the eGf event. The observed waveforms are well explained by the theoretical waveforms at almost every station. The variance reduction (V.R.) of the data is calculated as a measure of the fit between two seismogram traces, such that

$$\text{V.R.} = \sum_{t,j}\left(\dot{u}_j^{obs}(t) - \dot{u}_j^{cal}(t)\right)^2 / \sum_{t,j}\left(\dot{u}_j^{obs}(t)\right)^2, \tag{8}$$

where $\dot{u}_j^{obs}(t)$ and $\dot{u}_j^{cal}(t)$ represent the theoretical waveform and the observed waveform at the jth station, respectively. The V.R. was 87% for M2005.

Figure 5 shows the total slip distribution and slip rate history for M2005. The initial M2005 rupture (in the snapshot at 0.1 s) was near the D2005 source location, with the rupture then propagating bilaterally and parallel to the slip direction (Fig. 5c). We emphasize again that the initial rupture point and rupture velocity are not constrained in this inversion. Our modeled magnitude of M2005 is *Mw*4.7, which is close to the *M*4.8 value estimated by JMA. The largest amount of slip occurs near the source area of the eGf event, where the total slip is 40–70 cm. This estimated slip is comparable with the expected slip deficit of 43–51 cm, which was calculated from the plate subduction rate of 8.5 cm/yr and the recurrence interval of 5–6 years for the M events.

The result shown in Fig. 5 depends on the specific eGf event; however, near-identical results were obtained using other eGf events. Additional file 1: Figure S2 shows the result when D2009 is used as the eGf event, where a qualitatively similar rupture history and slip distribution are observed.

The slip inversions of the M2010 and M2016 events, where D2005 was used as the eGf event, had V.R. values of 87 and 90%, respectively, with estimated earthquake magnitudes of 4.6 and 4.5, which were slightly smaller than the JMA catalog magnitudes of 4.8 and 4.7, respectively. M2010 and M2016 follow a similar rupture propagation process (Additional file 1: Figures S3 and S4, respectively), with the rupture initiating ~500 m shallower than the D2005 source location and propagating in the down-dip direction after rupturing the area near the D2005 source location. The total slip distributions of M2010 and M2016 are elongate in the slip direction. The largest amounts of slip occur near the source area of the eGf event, where the total slips are 50–60 cm for each event. These estimated slips are comparable with the expected slip deficit of 43–51 cm. However, the simple source mechanism of D2009 (Additional file 1: Figure S5), which is approximated by a point source near the

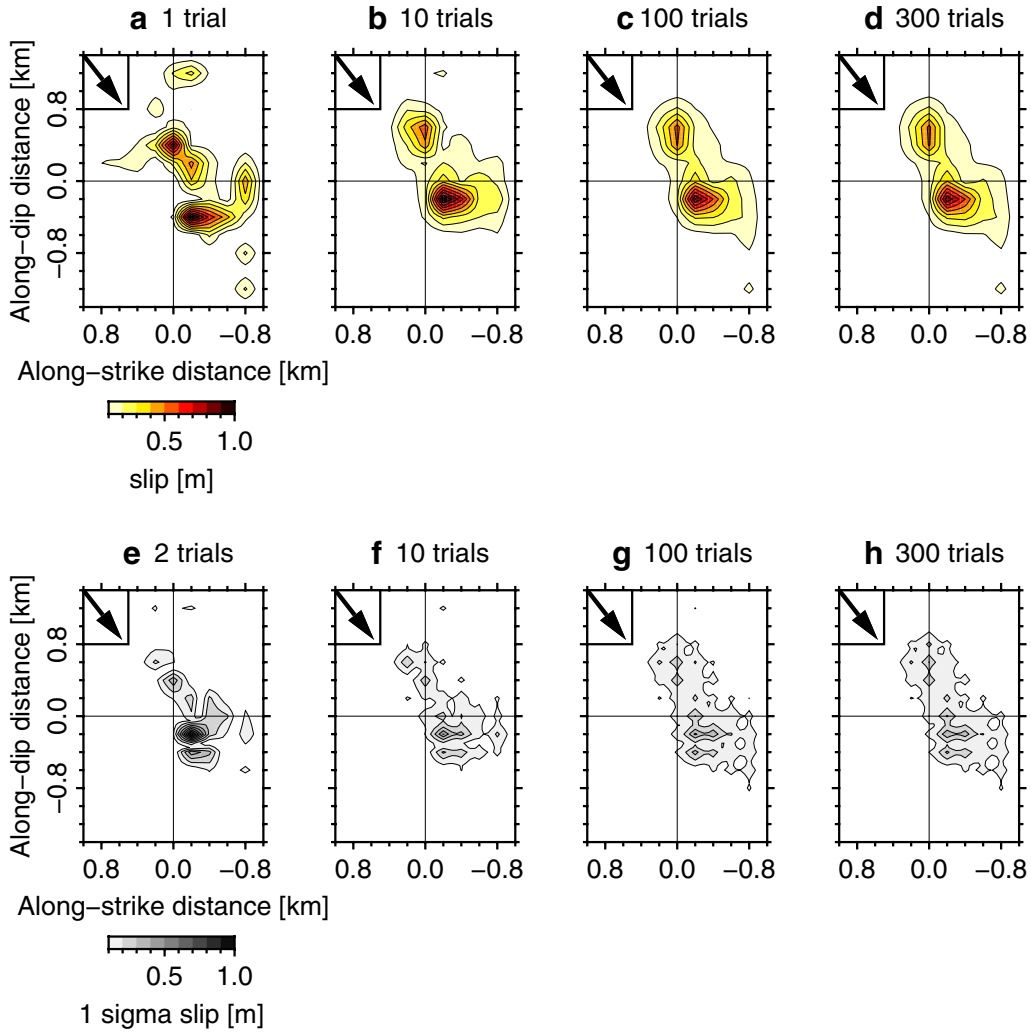

Fig. 3 Bootstrap method. The total slip distribution of M2005 in the Kushiro-Oki region after **a** 1 **b** 10, **c** 100, and **d** 300 trials. The standard deviation of slip distribution after (**e**) 2, (**f**) 10, (**g**) 100, and (**h**) 300 trials. The contour interval is 10 cm. The black arrow at upper left shows the slip direction from the F-net data.

Table 1 Kushiro-Oki earthquakes

Name	Group	Year	Month	Day	Hour	Minute	Magnitude	
D2005	D	2005	4	14	9	25	2.8	EGF1
M2005	M	2005	5	19	1	33	4.8	
D2009	D	2009	10	15	17	11	2.7	EGF2
M2010	M	2010	4	9	3	41	4.8	
M2016	M	2016	3	30	14	9	4.7	

The source time of each event is from the JMA catalog. EGF1 and EGF2 signify the events used as eGf events in this study

D2005 source location, exhibits no such elongation of the slip distribution.

A summary of the total slip distributions of the four earthquakes in the Kushiro-Oki region, projected onto common spatial coordinates, is shown in Fig. 6. The M2005 slip area is more elongate in the shallower region of the fault plane than those of the other group M events. This difference may be due to the afterslip of the 2003

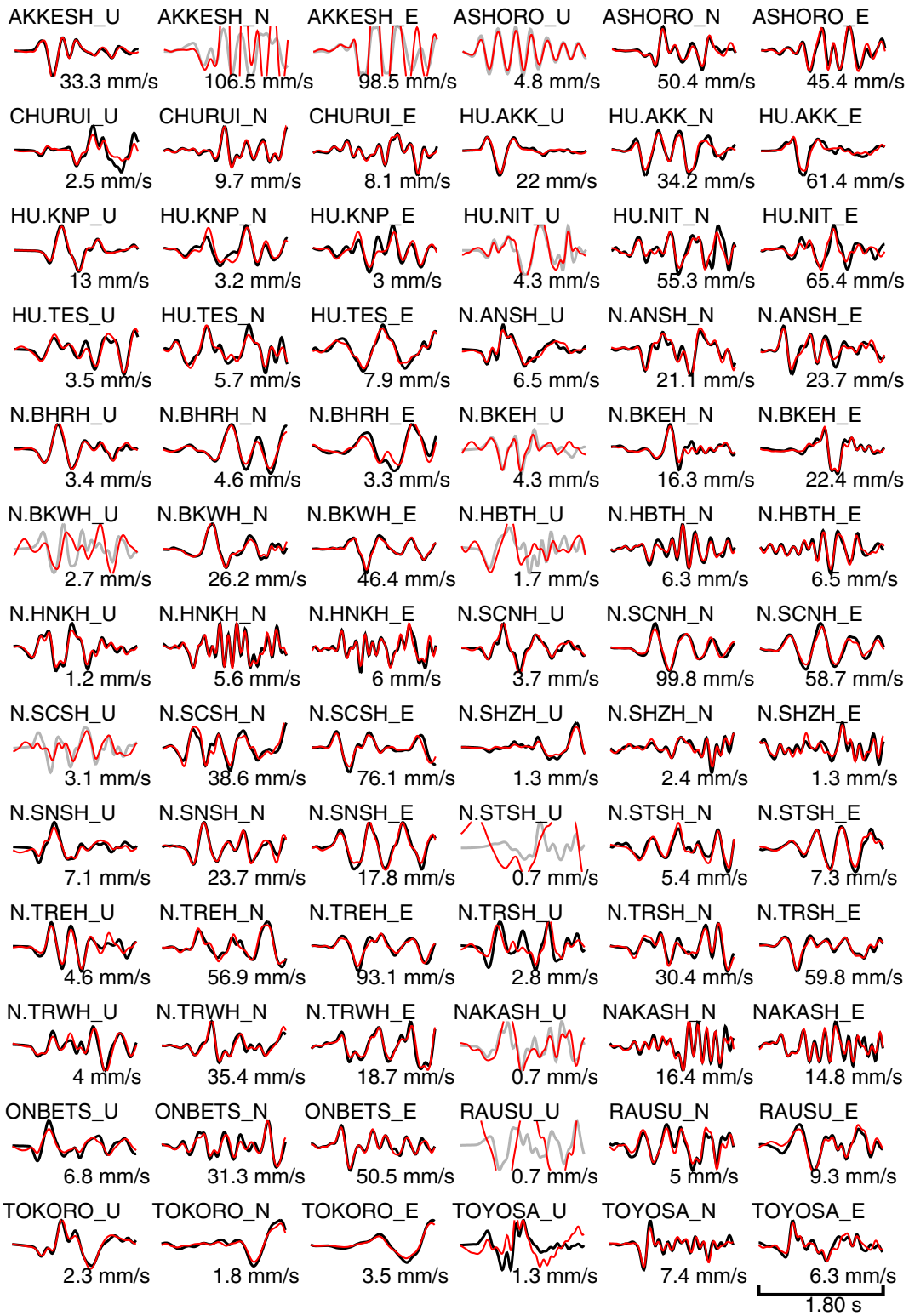

Fig. 4 Comparison between the observed (black lines) and synthetic (red lines) seismograms for M2005. The gray lines indicate unused (noisy) data. Each set of traces is normalized by the maximum value of the observed seismograms, which is listed at the bottom of each seismogram

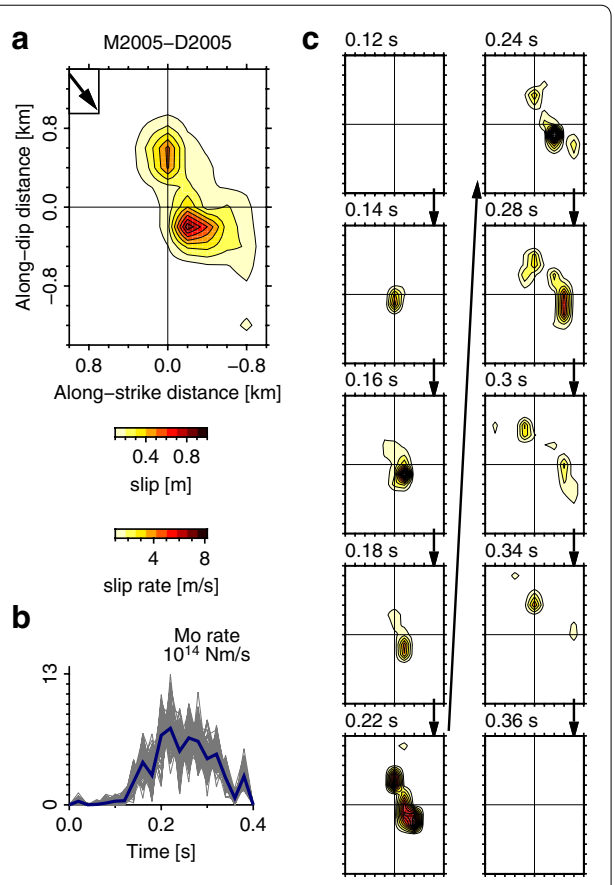

Fig. 5 M2005 source process. **a** Total slip distribution. The down direction in the figure indicates the down-dip direction,and the black arrow at upper left shows the slip direction from the F-net data.The origin indicates the D2005 source location (eGf event). **b** Moment rate function, with the gray lines representing each trial and the blue line being the average. **c** Slip rate history. The modeled region in (**c**) is the same as in (**a**)

*Mw*8.3 Tokachi-Oki earthquake on the shallower part of the same plate interface (Koketsu et al. 2004), since expansion of the slip area of repeating earthquakes has also been reported in the Kamaishi-Oki region after the 2011 *Mw*9.0 Tohoku-Oki earthquake (e.g., Uchida et al. 2015). The rupture areas of the three moderate-size repeating earthquakes (M2005, M2010, and M2016) overlap and are elongate parallel to the slip direction, with the exception of this shallower area. A part of these areas was also repeatedly ruptured by smaller events (D2005 and D2009).

Results of the Naka-Oki slip inversion

We determined the spatiotemporal slip distribution of the five *M*4.7–4.8 earthquakes and four smaller group A and B earthquakes (Table 2, Additional file 1: S5) in the Naka-Oki region. A comparison between the observed and modeled M2015 waveforms is shown in Additional file 1: Figure S6, with B2007 used as the eGf event. The observed waveforms are well explained by the theoretical waveforms at almost every station, yielding a V.R. value of 86% for M2015. Figure 7 shows the total slip distribution and slip rate history, where the rupture of M2015 initiated near the B2007 source location and then propagated bilaterally and parallel to the slip direction (Fig. 7c). The M2015 magnitude is *Mw*4.8, which is close to the *M*4.8 estimated by JMA. Almost identical results were obtained using other eGf events, with the result using B2011 as the eGf event shown in Additional file 1: Figure S7.

The slip inversions of the other major events (M2003, M2007, M2011, and M2013), where B2007 was used as the eGf event, had V.R. values of 76, 90, 89, and 86%, respectively, with estimated earthquake magnitudes of 4.7, 4.7, 4.8, and 4.9, which are consistent with the JMA catalog magnitudes of 4.7, 4.7, 4.8, and 4.8, respectively. These earthquakes had complex and variable rupture processes that included the initial rupture location and directivity of each event rupture. While some of the earthquake ruptures initiated shallower than the B2007 source location and the rupture propagated unilaterally, the others initiated near the B2007 source location and the rupture propagated bilaterally (Additional file 1: Figures S8–S11). Such a complex rupture process is true for both the major $M\sim4.8$ events and the three $M\sim4$ events (A2007, A2010, and A2012; Additional file 1: Figures S12–S14). The total slip distributions of all the group M and A events are elongate in the slip direction. However, the simplified source mechanism of B2011, which was approximated by a point source near the B2007 source location, yielded no elongation of the slip distribution (Additional file 1: Figure S15).

A maximum slip of 70–110 cm is observed in the slip distributions of M2007, M2011, and M2015, which occurs near the source area of the eGf event. These values are much larger than the estimated slip deficit of 26–43 cm, which is calculated from the plate subduction rate of 8.5 cm/yr and the recurrence interval for group M earthquakes of 3–5 years. This discrepancy implies that the actual slip may be more spatially smoothed. As mentioned above, we did not use smoothing to spatially constrain the slip distribution, such that the estimated slip tends to be locally concentrated.

A summary of the total slip distributions of the nine analyzed Naka-Oki earthquakes, projected onto common spatial coordinates, is shown in Fig. 8. The rupture areas of the five moderate-size repeating earthquakes overlap and are elongate parallel to the slip direction. A portion of this rupture area was also repeatedly ruptured by smaller events (A2007, A2010, B2011, and B2007). The rupture area of A2012 expanded outside the rupture

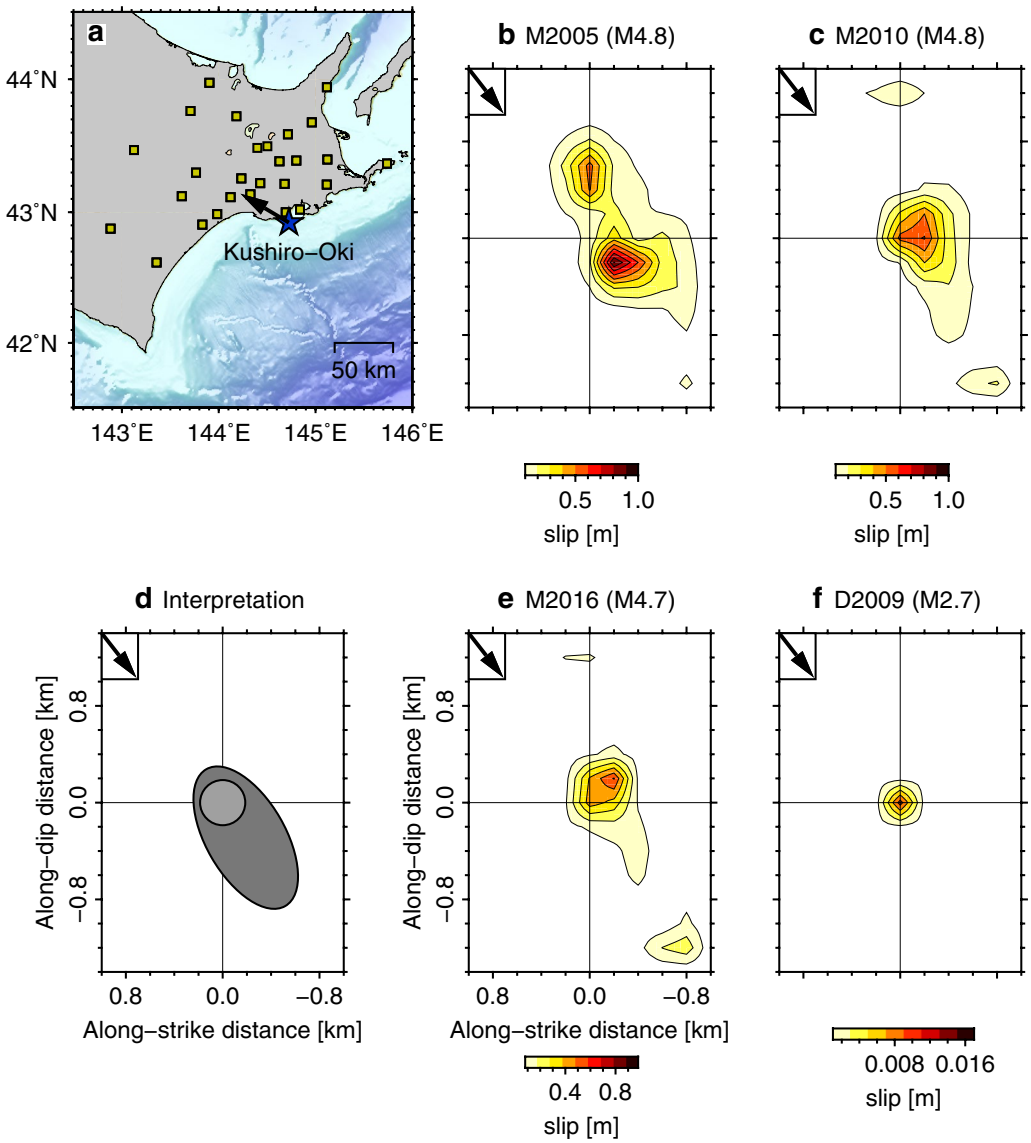

Fig. 6 Total slip distributions of the Kushiro-Oki earthquakes. **a** Map showing the locations of the stations (yellow squares) used in the waveform inversion, relative to the Kushiro-Oki events (blue star), with the slip direction indicated by the black arrow. Total slip distributions of M2005 **b**, M2010 **c**, M2016 **e**, and D2009 **f**, projected onto common spatial coordinates. **d** Interpretation of the characteristic structure represented by two patches elongate in the slip direction on the plate interface in the Kushiro-Oki region

area of the other Naka-Oki events. Although this might look odd, the error estimated by bootstrapping method is sufficiently small (Additional file 1: Figure S16 h), suggesting the validity of the result. Except for this point, the rupture areas of the two $M \sim 4$ earthquakes (A2007 and A2010) overlap and are elongate parallel to the slip direction. The rupture areas of the group B events correspond to part of the rupture areas of the group M and A events.

Characteristics of the rupture process

Characteristics of rupture phenomena

Every moderate-size repeating earthquake has complex and variable rupture processes that include the initial rupture location and directivity of the event rupture (Figs. 5, 7, Additional file 1: S3, S4, S8–S15). Nevertheless, most of their rupture areas overlap significantly (Figs. 6 and 8), with some parts of these areas also being

Table 2 Naka-Oki earthquakes

Name	Group	Year	Month	Day	Hour	Minute	Magnitude	
M2003	M	2003	6	9	9	18	4.7	
A2007	A	2007	5	18	17	2	3.9	
B2007	B	2007	6	3	6	48	2.9	EGF1
M2007	M	2011	11	30	18	36	4.7	
A2010	A	2010	4	29	7	21	4.2	
B2011	B	2011	8	29	12	45	2.9	EGF2
M2011	M	2011	9	10	15	0	4.8	
A2012	A	2012	12	6	19	17	4.3	
M2013	M	2013	10	12	2	43	4.8	
M2015	M	2015	11	22	8	20	4.8	

The source time of each event is from the JMA catalog. EGF1 and EGF2 signify the events used as eGf events in this study

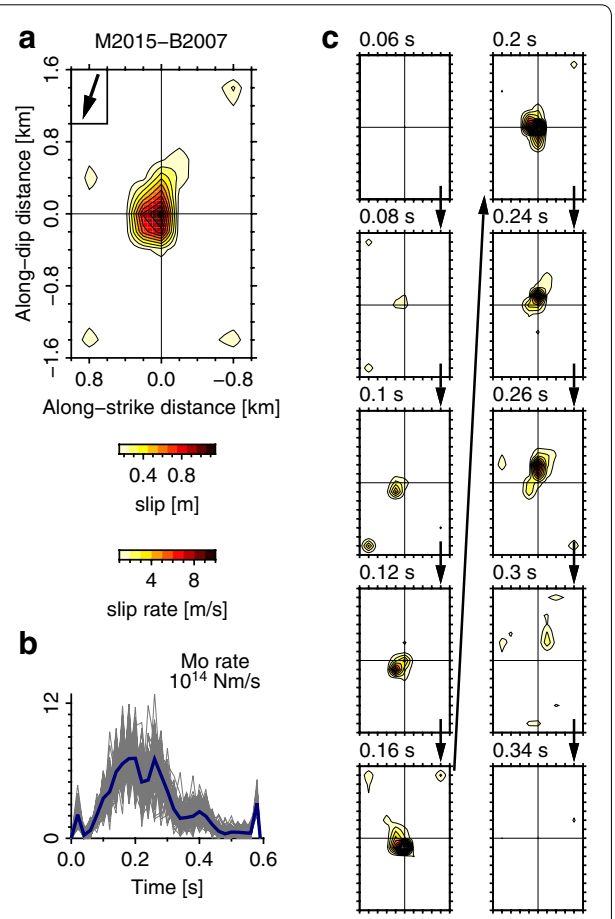

Fig. 7 M2015 source process. **a** Total slip distribution. The down direction in the figure indicates the down-dip direction, and the black arrow at upper left shows the slip direction from the F-net data.The origin indicates the B2007 source location (eGf event). **b** Moment rate function. The gray lines represent each trial, and the blue line is the average. **c** Slip rate history. The modeled region in (**c**) is the same as in (**a**)

repeatedly ruptured by smaller earthquakes. The $M\sim3$ and $M\sim4$ earthquakes in the Naka-Oki region and the $M\sim3$ events in the Kushiro-Oki region ruptured part of the rupture areas of the mainshocks in each region.

The M2005 and A2012 rupture areas expanded beyond the slip region of the similar-size earthquakes (Figs. 6, 8). These exceptions might be due to the effect of post-seismic process after large earthquakes, i.e., the 2003 Tokachi-Oki earthquake (*Mw*8.3) and the 2011 Tohoku-Oki earthquake (*Mw*9.0), respectively. In the Kushiro-Oki region, the 2003 Tokachi-Oki earthquake is followed by large afterslip, which triggered the 2004 Kushiro-Oki earthquake of M7.1 (Uchida et al. 2009). Therefore, it is likely that M2005 was also influenced by the afterslip. Similarly, the extended rupture area of A2012 may be due to the afterslip of the 2011 *Mw*9.0 Tohoku-Oki earthquake on the shallower part of the same plate interface (Ozawa et al. 2011), since the aseismic-to-seismic transition in slip behavior has previously been reported in the Tohoku-Oki region after the 2011 Tohoku-Oki earthquake (Uchida et al. 2015; Hatakeyama et al. 2017). The effect of the Tohoku-Oki earthquake may be also responsible to the relatively large slip of M2011 compared to other group M earthquakes (Fig. 8).

These results suggest the existence of essentially time-independent patch-like structures that ruptured repeatedly in a characteristic manner (Figs. 6f, 8k). The patches with different sizes may possess a hierarchical distribution. The rupture of a small patch alone is recognized as a small earthquake, while a large earthquake is the result of the continued rupture on increasingly larger patches. The difference between these small and large earthquakes may depend on subtle differences in the physical conditions surrounding the patches.

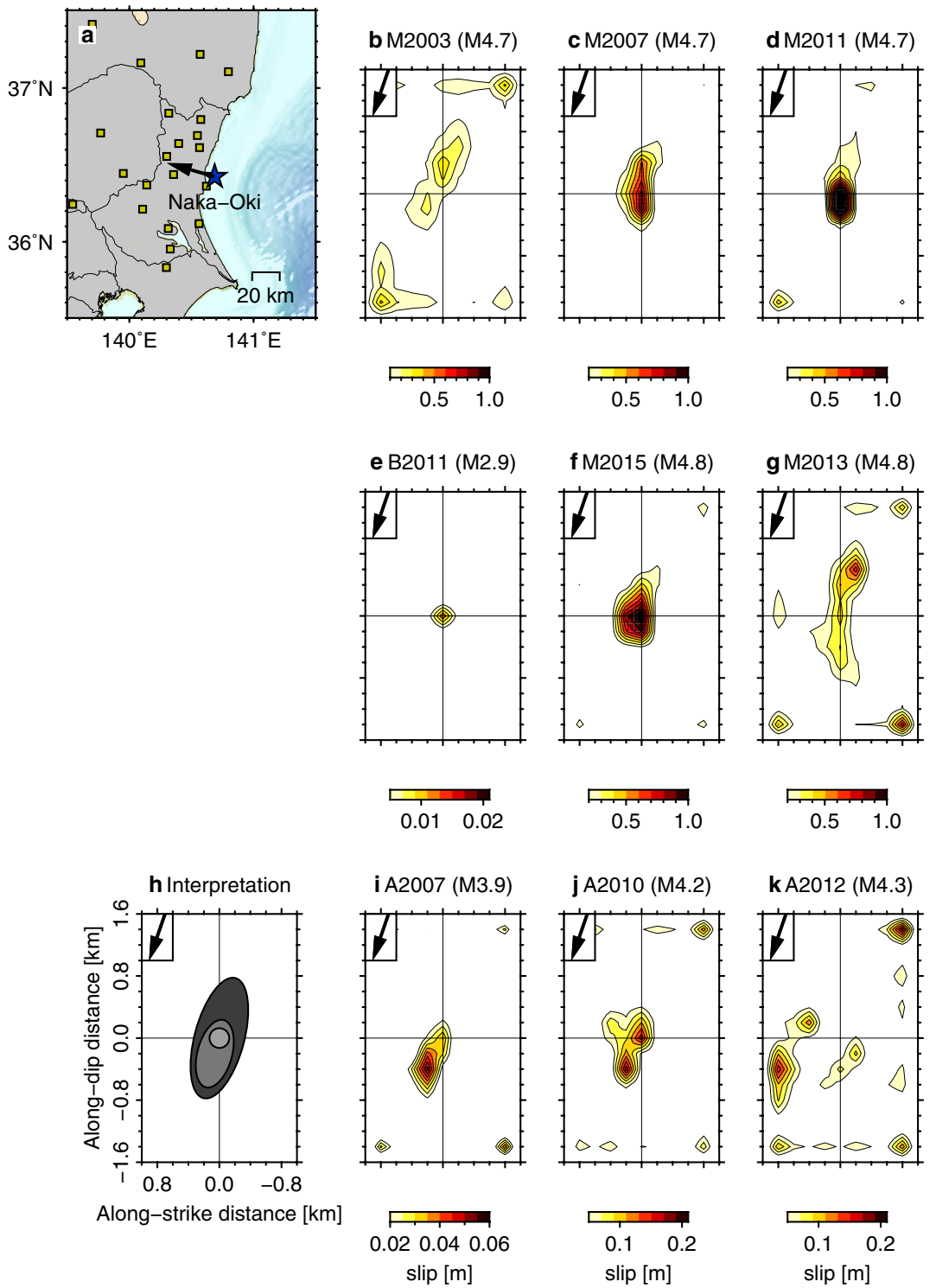

Fig. 8 Total slip distributions of the Naka-Oki earthquakes. **a** Map showing the locations of stations (yellow squares) used in the waveform inversion, relative to the Naka-Oki events (blue star), with the slip direction indicated by the black arrow. The total slip distributions of M2003 (**b**), M2007 (**c**), M2011 (**d**), M2013 (**g**), M2015 (**f**), B2011 (**e**), A2007 (**i**), A2010 (**j**), and A2012 (**k**), projected onto common spatial coordinates. **h** Interpretation of the characteristic structure represented by three patches elongate in the slip direction on the plate interface in the Naka-Oki region

Elongate slip distribution

Our results suggest either some linear structure that extends in the slip direction or the long-term motion along the plate boundary. Almost all the $M>4$ earthquakes in the Naka-Oki and Kushiro-Oki regions possess a slip distribution that is elongate in the slip direction. However, the heterogeneous azimuthal station distribution, with most of the stations to one side of the events, may suggest that this elongation is an artifact. The 1-σ model error is estimated to be three times smaller than the estimated value (Additional file 1: Figures S16 and S17), which indicates that the slip anisotropy of these earthquakes is not an artifact. Furthermore, the total slip distribution of the $M\sim3$ earthquakes in each region is estimated as an approximate point source without any elongation (Figs. 6e, 8g). Moreover, the elongation direction is in parallel to the slip direction, rather than the dip direction, which is more likely to appear as the result of inhomogeneous station distribution. The station distributions are quite different between the Kushiro-Oki and Naka-Oki regions. Therefore, it is unlikely that the modeled elongation is an artifact due to this heterogeneous station distribution. We propose that this elongate slip distribution that is parallel to the slip direction is a common feature of earthquakes in the Tohoku–Hokkaido subduction zone. This interpretation is supported by the slip distributions of larger earthquakes, such as the 2003 Tokachi-Oki (*Mw*8.3) and 2005 Miyagi-Oki (*Mw*7.2) earthquakes, which were also elongate in the slip direction (Koketsu et al. 2004; Yaginuma et al. 2007; Wu et al. 2008).

This similarity is also apparent in the seismicity. The earthquakes in the Urakawa-Oki and Kamaishi-Oki regions show linear distributions in the slip direction (Fig. 1c, d). A similar observation has also been reported for the strike-slip environment of the San Andreas Fault, California, where Rubin and Gillard (2000) showed linear distributions of small repeating earthquakes. The elongate slip distributions and linear earthquake distributions are probably different manifestations of the anisotropy in the slip direction. We therefore return to the idea of a patchy structure. If several patches are sparsely distributed in the slip direction, then each patch tends to rupture independently, as observed in the Urakawa-Oki and Kamaishi-Oki regions. However, if several patches are densely distributed in the slip direction, each patch tends to rupture dynamically and continuously, following the observations in the Kushiro-Oki and Naka-Oki regions. Field observations from outcropping faults have reported that a characteristic structure develops in the slip direction, with the fault surfaces corrugated on a variety of scales and possessing lineations that are parallel to the slip direction (Power et al. 1987, 1988; Power and Tullis 1991; Kuwahara et al. 1993; Lee and Bruhn 1996; Renard et al. 2006; Candela et al. 2009; Kirkpatrick and Brodsky 2014). The patchy structure must therefore be related to these field observations.

The Japan Trench shows a distinctive faulting pattern that consists of horst–graben structures (Ludwig et al. 1966; Kobayashi et al. 1998; Tsuru et al. 2000; Nakamura et al. 2013). The bending of the oceanic plate in the subduction zone causes many normal faults at the outer rise of the trench, where horst–graben structures form parallel to the trench axis (Jones et al. 1978; Hilde 1983). However, our results show that the characteristic structure is parallel to the slip direction, which is almost perpendicular to the trench axis. This discrepancy indicates that the direction of the characteristic structure changes from the trench axis direction in the shallower part of the plate boundary to the slip direction in the deeper part during the long-term subduction process.

It is important to identify how the structure of the plate boundary regulates earthquake behavior to better understand the physical mechanisms that influence the occurrence of earthquakes. Our results suggest that a streak structure in the slip direction regulates the earthquake slip distribution along the 1000 km along-strike section of the Tohoku–Hokkaido subduction zone, extending from Kushiro-Oki to Naka-Oki region. The error tends to be large parallel to the slip or dip directions of the subducting slab due to the limited station coverage in the offshore region. Therefore, it would be difficult to discuss the anisotropy of the slip distribution from offshore events. A detailed quantitative and statistical discussion will be possible after the homogeneous station coverage obtained after the addition of the Seafloor Observation Network for Earthquakes and Tsunamis along the Japan Trench (S-net), which has started full-scale operations from April 2017 (Mochizuki et al. 2016).

Hierarchical rupture growth

A comparison of the rupture processes between M2007 (*M*4.8) and A2010 (*M*4.2) is shown in Fig. 9. The raw velocity waveforms are shown in Fig. 9a, where the relative arrival time differences at each station are preserved, with no filtering or normalization of the seismograms. The near-identical P-wave onsets indicate that the M2007 and A2010 ruptures originated from approximately the same location. Their waveforms are also indistinguishable during the first 0.1 s. This initial waveform similarity indicates that these processes initiate with a near-identical rupture process during the first 0.1 s. Figure 9b compares their slip rate histories, with near-identical rupture processes observed in the first 0.1 s. However, the differences in their rupture processes become clear after 0.12 s.

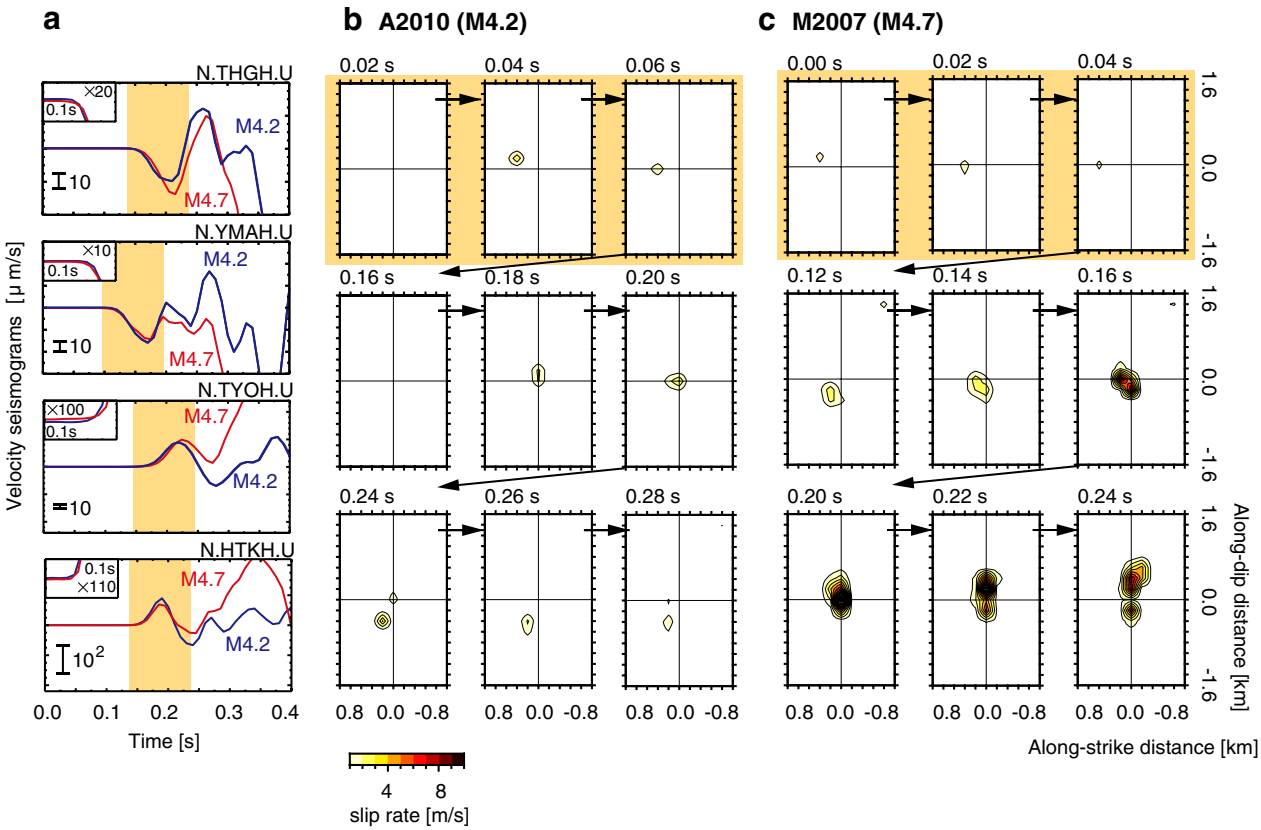

Fig. 9 Comparison between the M2007 (*M*4.8) and A2010 (*M*4.2) events. **a** The vertical components of the raw velocity seismograms for M2007 and A2010, with the onset of the P-wave responses magnified in the inset. The orange zones mark the 0.1-s time interval where the larger and smaller events possess similar initial seismic responses. Slip rate histories for **b** M2007 and **c** A2010, projected onto common spatial coordinates. The highlighted slip history panels indicate the near-identical early slip histories

The A2010 slip rate decreases gradually, while the M2007 slip rate accelerates and grows into a larger event.

Near-identical initial waveforms were observed for several combinations of small and large earthquakes in the Kushiro-Oki and Naka-Oki regions (Additional file 1: Figure S18). These examples indicate that when a small rupture occurs, the rupture may soon decelerate and stop, producing only a small earthquake, or it may grow into a large earthquake. This specific rupture process is dependent on subtle differences in the physical conditions of the fault interface, which appear to be random practically. Figure 10 illustrates these processes, where the fault interface consists of a series of hierarchical patches. The patches are elliptical and elongate in the slip direction, as described in the previous section. A large strong patch with a large fracture energy contains smaller weak patches, with the initial rupture tending to nucleate on these smaller patches. The failure of a small patch may trigger the failure of a larger patch, which is sometimes called the "cascade-up" process in numerical simulations (Noda et al. 2013) and rock experiments (Mclaskey et al. 2014). A large earthquake in this model is the result of successive cascade-up processes from a tiny patch to a giant patch.

These near-identical waveforms conceptually correspond to the repetitive rupture of the same single fault (e.g., Nadeau and Johnson 1998; Nadeau and McEvilly 1999). However, the real plate boundary is a geometrically complex structure that includes branch faults as off-plane faults (Tchalenko and Ambraseys 1970; Swanson 2006; Hamling et al. 2017). It is unlikely that a rupture over several hundred meters repeats in exactly the same way. Therefore, the same area of the fault may not be reactivated during these repetitive rupture processes, making it necessary to consider a space that includes a fault cluster. This fault cluster will undergo a successive and simultaneous rupture process when the stress reaches its yield limit, such that it may behave like a single rupture unit due to the dynamic triggering process. Such a rupture unit may be viewed as a repeating earthquake that generates identical seismic waveforms.

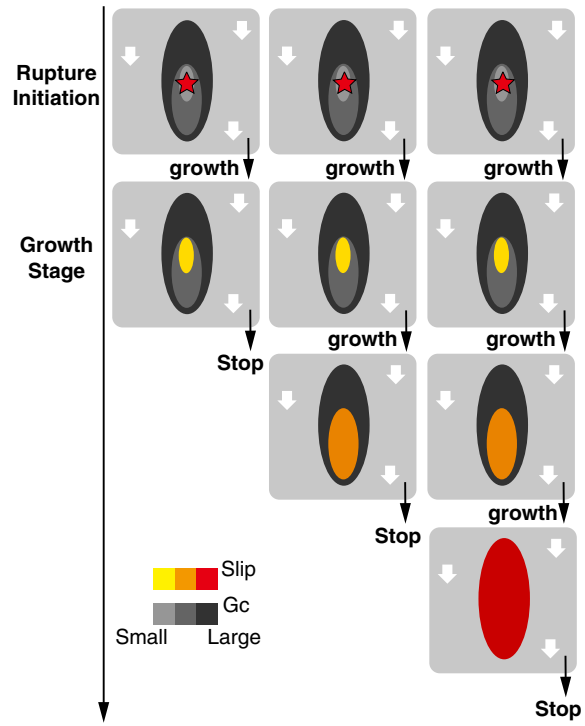

Fig. 10 Conceptual hierarchical patch model. The hierarchical structure, which is defined by the different patch sizes in the figure, controls the overall earthquake behavior. A large earthquake can be interpreted as the result of a cascade-up process that initiated from a small-patch rupture. The patches are elliptical and elongate in the slip direction

Conclusion

There has been considerable debate whether the size of an earthquake can be characteristically determined or if it is a random process in a given seismic region. These are the two end-members that define an earthquake rupture process, each of which is conceptually represented by the hierarchical and characteristic models. Most earthquakes probably have intermediate properties that are highly variable. However, the earthquake occurrence model remains qualitative due to insufficient observations of repetitive ruptures in specific study regions. We therefore investigated several moderate-size repeating earthquakes as ideal targets to better understand these rupture processes.

We investigated four families of moderate-size ($M \sim 4.8$) repeating earthquakes and nearby smaller events in the Tohoku–Hokkaido subduction zone, Japan, between 2002 and 2017, using a hypocenter relocation method and a waveform inversion method. The rupture areas of the moderate-size repeating earthquakes overlapped significantly and were elongate parallel to the slip direction. Some parts of these areas were also repeatedly ruptured by smaller earthquakes. These smaller earthquakes and moderate events sometimes followed near-identical rupture processes.

These results suggest the existence of an essentially time-independent characteristic streak structure that is represented by several elliptical patches that are elongate in the slip direction of the plate interface. These patches may possess a hierarchical distribution, where a large earthquake is the failure of a large patch, which is the consequence of successive cascade-up processes from a small patch. The small patch may also host an independent smaller earthquake. The potential for a small-patch rupture to grow into a large-scale rupture depends on subtle differences in the physical conditions of the slip interface, which we cannot observe in a practical sense. Similar structures may have developed along the 1000-km section of the subduction zone, extending from Hokkaido to the Kanto region, which play an important role in the earthquake rupture process. Earthquakes are random processes, but they may not be completely random, as preexisting characteristics of the seismogenic region regulate the earthquake rupture behavior to some degree. It is therefore useful to identify the hierarchical and streak structures for each seismogenic region to better predict the size of a given earthquake.

Additional file

Additional file 1. Tables S1–S5 and Figures S1–S18.

Authors' contributions

TO made waveform analysis and wrote most of the manuscript including figures. SI planned research and prepared analysis tools. Both authors read and approved the final manuscript.

Acknowledgements

We thank T. Nishikawa and D. Sato for discussions, and N. Uchida for providing the repeating earthquake catalog. Comments from two anonymous reviewers helped to improve the manuscript.

Competing interests

The authors declare that they have no competing interests.

Availability of data and materials

All waveform data and JMA hypocenter catalog are available at NIED Hi-net server http://www.hinet.bosai.go.jp.

Funding

This study was supported by the Ministry of Education, Culture, Sports, Science and Technology (MEXT) of Japan, under its Earthquake and Volcano Hazards Observation and Research Program, JSPS KAKENHI 16H02219, and MEXT KAKENHI 16H06477.

Publisher's Note

Received: 3 April 2018 Accepted: 2 August 2018
Published online: 13 August 2018

References

Abercrombie R, Mori J (1994) Local observations of the onset of a large earthquake—28 June 1992 Landers, California. Bull Seismol Soc Am 84:725–734

Aki K, Richards PG (1980) Quantitative seismology: theory and methods. W. H. Freeman, New York

Bakun WH, Lindh AG (1985) The Parkfield, California, earthquake prediction experiment. Science 229:619–624. https://doi.org/10.1126/science.229.4714.619

Bakun WH, Aagaard B, Dost B et al (2005) Implications for prediction and hazard assessment from the 2004 Parkfield earthquake. Nature 437:969–974. https://doi.org/10.1038/nature04067

Candela T, Renard F, Bouchon M et al (2009) Characterization of fault roughness at various scales: implications of three-dimensional high resolution topography measurements. Pure appl Geophys 166:1817–1851. https://doi.org/10.1007/s00024-009-0521-2

Chen KH, Nadeau RM, Rau RJ (2008) Characteristic repeating earthquakes in an arc-continent collision boundary zone: the Chihshang fault of eastern Taiwan. Earth Planet Sci Lett 276:262–272. https://doi.org/10.1016/j.epsl.2008.09.021

Efron B, Tibshirani RJ (1994) An introduction to the bootstrap. CRC Press, Boca Raton

Ellsworth WL, Beroza GC (1995) Seismic evidence for an earthquake nucleation phase. Science 268:851–855. https://doi.org/10.1126/science.268.5212.851

Gutenberg B, Richter CF (1944) Frequency of earthquakes in California. Bull Seismol Soc Am 34:185–188

Hamling IJ, Hreinsdóttir S, Clark K et al (2017) Complex multifault rupture during the 2016 Mw 7.8 Kaikōura earthquake, New Zealand. Science. https://doi.org/10.1126/science.aam7194

Hatakeyama N, Uchida N, Matsuzawa T, Nakamura W (2017) Emergence and disappearance of interplate repeating earthquakes following the 2011 *M* 9.0 Tohoku-oki earthquake: slip behavior transition between seismic and aseismic depending on the loading rate. J Geophys Res Solid Earth 122:5160–5180. https://doi.org/10.1002/2016JB013914

Hilde TWC (1983) Sediment subduction versus accretion around the pacific. Tectonophysics 99:381–397. https://doi.org/10.1016/0040-1951(83)90114-2

Ide S (2001) Complex source processes and the interaction of moderate earthquakes during the earthquake swarm in the Hida-Mountains, Japan, 1998. Tectonophysics 334:35–54. https://doi.org/10.1016/S0040-1951(01)00027-0

Ide S, Aochi H (2005) Earthquakes as multiscale dynamic ruptures with heterogeneous fracture surface energy. J Geophys Res Solid Earth 110:1–10. https://doi.org/10.1029/2004JB003591

Ide S, Beroza GC (2001) Does apparent stress vary with earthquake size? Geophys Res Lett 28:3349–3352

Ide S, Takeo M (1997) Determination of constitutive relations of fault slip based on seismic wave analysis. J Geophys Res Solid Earth 102:27379–27391. https://doi.org/10.1029/97JB02675

Igarashi T (2010) Spatial changes of inter-plate coupling inferred from sequences of small repeating earthquakes in Japan. Geophys Res Lett 37:1–5. https://doi.org/10.1029/2010GL044609

Igarashi T, Matsuzawa T, Hasegawa A (2003) Repeating earthquakes and interplate aseismic slip in the northeastern Japan subduction zone. J Geophys Res Solid Earth 108:1–9. https://doi.org/10.1029/2002JB001920

Jones GM, Hilde TWC, Sharman GF, Agnew DC (1978) Fault patterns in outer trench walls and their tectonic significance. J Phys Earth 26:85–101

Kanamori H, Anderson DL (1975) Theoretical basis of some empirical relations in seismology. Bull Seismol Soc Am 65:1073

Kirkpatrick JD, Brodsky EE (2014) Slickenline orientations as a record of fault rock rheology. Earth Planet Sci Lett 408:24–34. https://doi.org/10.1016/J.EPSL.2014.09.040

Kobayashi K, Nakanishi M, Tamaki K, Ogawa Y (1998) Outer slope faulting associated with the western Kuril and Japan trenches. Geophys J Int 134:356–372. https://doi.org/10.1046/j.1365-246X.1998.00569.x

Koketsu K, Hikima K, Miyazaki S, Ide S (2004) Joint inversion of strong motion and geodetic data for the source process of the 2003 Tokachi-oki, Hokkaido, earthquake. Earth Planets Space 56:329–334

Kuwahara Y, Oyagi N, Takahashi H (1993) Topographic anistropy of slickenside from deep borehole sample and in an earthquake swarm region and its generation mechanism. Earth J Phys 41:75–85

Lawson CL, Hanson RJ (1984) Solving least squares problems. Prentice-Hall, Inc., Englewood Cliffs, New Jersey

Lee J-J, Bruhn RL (1996) Structural anisotropy of normal fault surfaces. J Struct Geol 18:1043–1059. https://doi.org/10.1016/0191-8141(96)00022-3

Ludwig WJ, Ewing JI, Ewing M et al (1966) Sediments and structures of the Japan Trench. J Geophys Res 71:2121–2137

Matsubara M, Yagi Y, Obara K (2005) Plate boundary slip associated with the 2003 Off-Tokachi earthquake based on small repeating earthquake data. Geophys Res Lett 32:1–4. https://doi.org/10.1029/2004GL022310

Matsumura S (2010) Discrimination of a preparatory stage leading to M7 characteristic earthquakes off Ibaraki Prefecture, Japan. J Geophys Res Solid Earth 115:1–14. https://doi.org/10.1029/2009JB006584

Matsuzawa T (2002) Characteristic small-earthquake sequence off Sanriku, northeastern Honshu, Japan. Geophys Res Lett 29:1543. https://doi.org/10.1029/2001GL014632

Mclaskey GC, Lockner DA (2014) Preslip and cascade processes initiating laboratory stick slip. J Geophys Res Solid Earth 119:6323–6336. https://doi.org/10.1002/2014JB011220.Received

Meier MA, Heaton T, Clinton J (2016) Evidence for universal earthquake rupture initiation behavior. Geophys Res Lett 43:7991–7996. https://doi.org/10.1002/2016GL070081

Menke W (2012) Geophysical data analysis: discrete inverse theory, MATLAB edition. Academic Press, San Diego, CA

Mochizuki K, Yamada T, Shinohara M et al (2008) Weak interface coupling by seamounts and repeating M ~ 7.0 earthquakes. Science 321:1194–1197. https://doi.org/10.1126/science.1160250

Mochizuki M, Kanazawa T, Uehira K, Shimbo T, Shiomi K, Kunugi T, Aoi S, Matsumoto T, Sekiguchi S, Yamamoto N, Takahashi N, Shinohara M, Yamada T (2016) S-net: Construction of large scale seafloor observatory network for tsunamis and earthquakes in Japan. AGU Fall Meeting 2016, NH43B-1840

Mori J, Kanamori H (1996) Initial rupture of earthquakes in the 1995 Ridgecrest, California sequence. Geophys Res Lett 23:2437–2440. https://doi.org/10.1029/96GL02491

Nadeau RM, Johnson LR (1998) Seismological studies at Parkfield VI: moment release rates and estimates of source parameters for small repeating earthquakes. Bull Seismol Soc Am 88:790–814

Nadeau RM, McEvilly TV (1999) Fault slip rates at depth from recurrence intervals of repeating microearthquakes. Science 285:718–721. https://doi.org/10.1126/science.285.5428.718

Nakamura Y, Kodaira S, Miura S et al (2013) High-resolution seismic imaging in the Japan Trench axis area off Miyagi, northeastern Japan. Geophys Res Lett 40:1713–1718. https://doi.org/10.1002/grl.50364

Noda H, Nakatani M, Hori T (2013) Large nucleation before large earthquakes is sometimes skipped due to cascade-up-Implications from a rate and state simulation of faults with hierarchical asperities. J Geophys Res Solid Earth 118:2924–2952. https://doi.org/10.1002/jgrb.50211

Ohta K, Ide S (2008) A precise hypocenter determination method using network correlation coefficients and its application to deep low-frequency earthquakes. Earth Planets Space 60:877–882. https://doi.org/10.1186/BF03352840

Ohta K, Ide S (2011) Precise hypocenter distribution of deep low-frequency earthquakes and its relationship to the local geometry of the subducting plate in the Nankai subduction zone, Japan. J Geophys Res Solid Earth 116:1–11. https://doi.org/10.1029/2010JB007857

Okada T, Matsuzawa T, Hasegawa A (2003) Comparison of source areas of M4.8 ± 0.1 repeating earthquakes off Kamaishi, NE Japan: are asperities persistent features? Earth Planet Sci Lett 213:361–374. https://doi.org/10.1016/S0012-821X(03)00299-1

Ozawa S, Nishimura T, Suito H, Kobayashi T, Tobita M, Imakiire T (2011) Coseismic and postseismic slip of the 2011 magnitude-9 Tohoku-Oki earthquake. Nature 475:373–375. https://doi.org/10.1038/nature10227

Peng Z, Ben-Zion Y (2005) Spatiotemporal variations of crustal anisotropy from similar events in aftershocks of the 1999 M7.4 Izmit and M7.1 Duzce, Turkey, earthquake sequences. Geophys J Int 160:1027–1043. https://doi.org/10.1111/j.1365-246X.2005.02569.x

Power WL, Tullis TE (1991) Euclidean and fractal models for the description of rock surface roughness. J Geophys Res 96:415. https://doi.org/10.1029/90JB02107

Power WL, Tullis TE, Brown SR et al (1987) Roughness of natural fault surfaces. Geophys Res Lett 14:29–32
Power WL, Tullis TE, Weeks JD (1988) Roughness and wear during brittle faulting. J Geophys Res Solid Earth 93:15268–15278. https://doi.org/10.1029/JB093iB12p15268
Renard F, Voisin C, Marsan D, Schmittbuhl J (2006) High resolution 3D laser scanner measurements of a strike-slip fault quantify its morphological anisotropy at all scales. Geophys Res Lett 33:L04305. https://doi.org/10.1029/2005GL025038
Rubin AM, Gillard D (2000) Aftershock asymmetry/rupture directivity among central San Andreas fault microearthquakes. J Geophys Res 105:19095. https://doi.org/10.1029/2000JB900129
Shimamura K, Matsuzawa T, Okada T et al (2011) Similarities and differences in the rupture process of the M ~ 4.8 repeating-earthquake sequence off Kamaishi, northeast Japan: comparison between the 2001 and 2008 events. Bull Seismol Soc Am 101:2355–2368. https://doi.org/10.1785/0120100295
Swanson MT (2006) Late paleozoic strike-slip faults and related vein arrays of Cape Elizabeth, Maine. J Struct Geol 28:456–473. https://doi.org/10.1016/j.jsg.2005.12.009
Tchalenko JS, Ambraseys NN (1970) Structural analysis of the Dasht-e Bayaz (Iran) earthquake fractures. Bull Geol Soc Am 81:41–60
Tsuru T, Park J, Takahashi N et al (2000) Tectonic features of the Japan Trench convergent margin off Sanriku, northeastern Japan, revealed by multichannel seismic reflection data. J Geophys Res 105:403–413
Uchide T, Ide S (2010) Scaling of earthquake rupture growth in the Parkfield area: self-similar growth and suppression by the finite seismogenic layer. J Geophys Res Solid Earth 115:1–15. https://doi.org/10.1029/2009JB007122
Uchida N, Matsuzawa T (2013) Pre- and postseismic slow slip surrounding the 2011 Tohoku-oki earthquake rupture. Earth Planet Sci Lett 374:81–91. https://doi.org/10.1016/j.epsl.2013.05.021
Uchida N, Yui S, Miura S, Matsuzawa T, Hasegawa A, Motoya Y, Kasahara M (2009) Quasi-static slip on the plate boundary associated with the 2003 M8.0 Tokachi-oki and 2004 M7.1 off-Kushiro earthquakes, Japan. Gondwana Res 16(3–4):527–533
Uchida N, Matsuzawa T, Ellsworth WL et al (2012) Source parameters of microearthquakes on an interplate asperity off Kamaishi, NE Japan over two earthquake cycles. Geophys J Int 189:999–1014. https://doi.org/10.1111/j.1365-246X.2012.05377.x
Uchida N, Shimamura K, Matsuzawa T, Okada T (2015) Postseismic response of repeating earthquakes around the 2011 Tohoku-oki earthquake: moment increases due to the fast loading rate. J Geophys Res Solid Earth 120:259–274. https://doi.org/10.1002/2013JB010933
Wu C, Koketsu K, Miyake H (2008) Source processes of the 1978 and 2005 Miyagi-oki, Japan earthquakes: repeated rupture of asperities over successive large earthquakes. J Geophys Res Solid Earth 113:1–15. https://doi.org/10.1029/2007JB005189
Yaginuma T, Okada T, Hasegawa A et al (2007) Coseismic slip distribution of the 2005 Miyagiof strong-motion and Teleseismic waveforms. Zisin (Journal Seismol Soc Japan 2nd Ser) 60:43–53. https://doi.org/10.4294/zisin.60.43
Yamanaka Y, Kikuchi M (2003) Source process of the recurrent Tokachi-oki earthquake on September 26, 2003 inferred from teleseismic body waves. Earth Planets Space 55:21–24. https://doi.org/10.1186/BF03352479
Yamanaka Y, Kikuchi M (2004) Asperity map along the subduction zone in northeastern Japan inferred from regional seismic data. J Geophys Res Solid Earth. https://doi.org/10.1029/2003JB002683
Yamashita Y, Shimizu H, Goto K (2012) Small repeating earthquake activity, interplate quasi-static slip, and interplate coupling in the Hyuga-nada, southwestern Japan subduction zone. Geophys Res Lett 39:1–5. https://doi.org/10.1029/2012GL051476